Wavelength-dependent spatial correction and spectral calibration of a liquid crystal tunable filter imaging system

Article *in* Applied Optics · April 2015

DOI: 10.1364/AO.54.003687

CITATIONS
5

READS
220

3 authors:

Roy S. Berns
Rochester Institute of Technology
249 PUBLICATIONS **5,843** CITATIONS
SEE PROFILE

Brittany Cox
Rochester Institute of Technology
3 PUBLICATIONS **7** CITATIONS
SEE PROFILE

Farhad Moghareh Abed
ON Semiconductor
15 PUBLICATIONS **75** CITATIONS
SEE PROFILE

applied optics

Wavelength-dependent spatial correction and spectral calibration of a liquid crystal tunable filter imaging system

Roy S. Berns,* Brittany D. Cox, and Farhad Moghareh Abed

Studio for Scientific Imaging and Archiving of Cultural Heritage, Program of Color Science, Rochester Institute of Technology, USA
**Corresponding author: berns@cis.rit.edu*

Received 9 December 2014; revised 18 March 2015; accepted 19 March 2015; posted 20 March 2015 (Doc. ID 227160); published 15 April 2015

The centroid wavelength of liquid crystal tunable filters (LCTFs), by definition, changes with incident angle, resulting in an imaging system with spectral sensitivity that varies across the image plane. Prior to this research, this effect was considered negligible. Imaging uniform colored papers with high chroma revealed that the effect is appreciable. A regression-based method of modeling and correcting systematic spectrophotometric errors in conventional reflectance spectrophotometry was used to correct this wavelength-dependent spatial nonuniformity in an LCTF imaging system. For six high chroma sheets of spatially uniform paper, the uniformity was reduced from an average and maximum of 0.95 and 4.00, respectively, to 0.08 and 0.18 CIEDE2000. The same method was used to transfer the scale of spectral reflectance factor from a reference spectrophotometer to the imaging system such that its reported values matched the reference spectrophotometer with a constant bandwidth. For an independent color target, residual errors were 0.008 spectral reflectance factor RMS difference and 0.44 and 1.65 average and maximum CIEDE2000, respectively (0.63 and 2.34 ΔE^*_{ab}).

OCIS codes: (110.4234) Multispectral and hyperspectral imaging; (300.6550) Spectroscopy, visible; (230.3720) Liquid-crystal devices.

http://dx.doi.org/10.1364/AO.54.003687

1. INTRODUCTION

Spectral imaging systems are readily constructed using a monochrome area-array sensor, spectrally selective filters, and appropriate collection optics. The filters can be, among others, a set of absorption or interference filters, an acoustic optic tunable filter, or a liquid crystal tunable filter (LCTF). The latter has the advantage of no moving parts, but the disadvantages of variable bandwidth and bandpass shape across wavelength and low throughput, particularly at shorter wavelengths [1]. For example, the spectral transmittance factor of a wide-bandwidth Cambridge Research & Instrumentation, Inc. (CRI) Varispec LCTF (circa 2000) is plotted in Fig. 1. These disadvantages are readily seen and typical of Varispec LCTFs from this time period [2].

The peak wavelength of both interference and LCTFs changes with incidence angle, and as a consequence, the spectral sensitivity of the imaging system will be spatially nonuniform. This spectral angular dependency is always considered negligible, and LCTF imaging systems are only corrected photometrically, for example in [3,4]. Using an incandescent light source reflected off a diffuse white surface or projected through an integrating sphere cannot reveal such dependency. By analogy, calibrated incandescent sources are never used to validate wavelength accuracy in a spectrometer. When the incident light is chromatic, the angular dependency is readily observed, demonstrated in Fig. 2 for an image of a spatially uniform red paper rendered from a LCTF spectral imaging system (described below). The colors in each corner mismatch one another and the center.

In our research, we use an LCTF-based imaging system as an imaging spectrophotometer. Accordingly, the scale of the spectral reflectance factor needs to be transferred from a reference spectrophotometer with constant bandwidth to the imaging system, and this transfer needs to occur across the entire image plane. This publication describes a methodology to correct the wavelength-dependent spatial nonuniformity and transfer the scale of the spectral reflectance factor from a reference spectrophotometer to an LCTF imaging system. More details are contained in Hensley and Wyble [5] and Abed and Berns [6].

2. THEORY

All spectrophotometers are subject to systematic and random errors [7], and common systematic errors include photometric scale errors, wavelength scale errors, and bandwidth errors [8]. Diagnosing and minimizing such errors can be performed using primary standards, such as line sources for wavelength error,

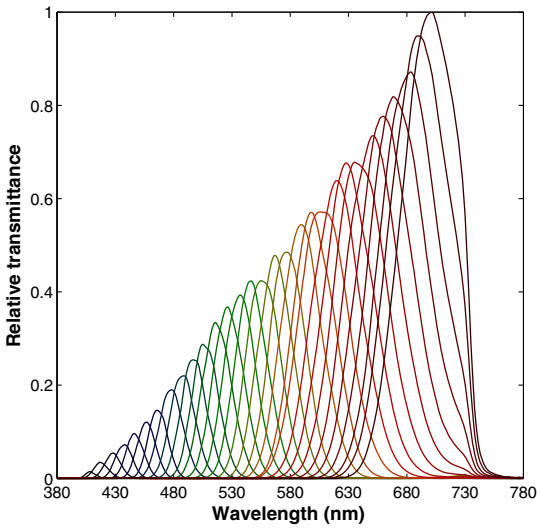

Fig. 1. Spectral transmittance factor of a wide-bandwidth CRI Varispec LCTF, circa 2000.

or secondary standards, such as achromatic and chromatic ceramic tiles where a standards laboratory transfers the spectral reflectance factor for a specific geometry [9]. Robertson [10] developed a tile-based method that was refined and tested by Berns and Petersen [11]. Errors were approximated as a linear model, and stepwise multiple-linear regression was used to diagnose and correct systematic differences between a specific spectrophotometer and a standards laboratory (or another spectrophotometer). Such a linear model is shown in Eq. (1) where $R_{\lambda,c}$ is the corrected spectral reflectance factor, $R_{\lambda,m}$ is the measured spectral reflectance factor, and $dR_{\lambda,m}/d\lambda$ and $dR^2_{\lambda,m}/d^2\lambda$ are the first and second derivatives of the measured spectral reflectance factor, respectively. Scalars β_0–β_2 correspond to zero, linear, and nonlinear photometric scale errors; β_3 corresponds to a linear wavelength error; and β_4 corresponds to a linear bandwidth error. Terms can be subtracted or added depending on the particular spectrophotometer as well as a function of wavelength, for instance a dispersing element with variable bandwidth. Moving $R_{\lambda,m}$ to the left side of Eq. (1), stepwise multiple-linear regression is used to select the statistically significant errors and estimate their model coefficients.

$$R_{\lambda,c} = R_{\lambda,m} - \beta_0 - \beta_1 R_{\lambda,m} - \beta_2(1 - R_{\lambda,m})R_{\lambda,m} - \beta_3 \frac{dR_{\lambda,m}}{d\lambda} - \beta_4 \frac{dR^2_{\lambda,m}}{d^2\lambda}. \quad (1)$$

For the specific case of an LCTF imaging system with i spectral bands where a sensor having pixel dimensions x and y outputs linear photometric data a, Eq. (1) becomes

$$a_{i,c,xy} = a_{i,xy} - \beta_{0,i,xy} - \beta_{1,i,xy} a_{i,xy} - \beta_{3,i,xy} \frac{da_{i,xy}}{d\lambda} - \beta_{4,i,xy} \frac{da^2_{i,xy}}{d\lambda}. \quad (2)$$

Each pixel of each spectral band can have a correction function. Equation (2) can be used to correct wavelength-dependent and independent spatial nonuniformities and

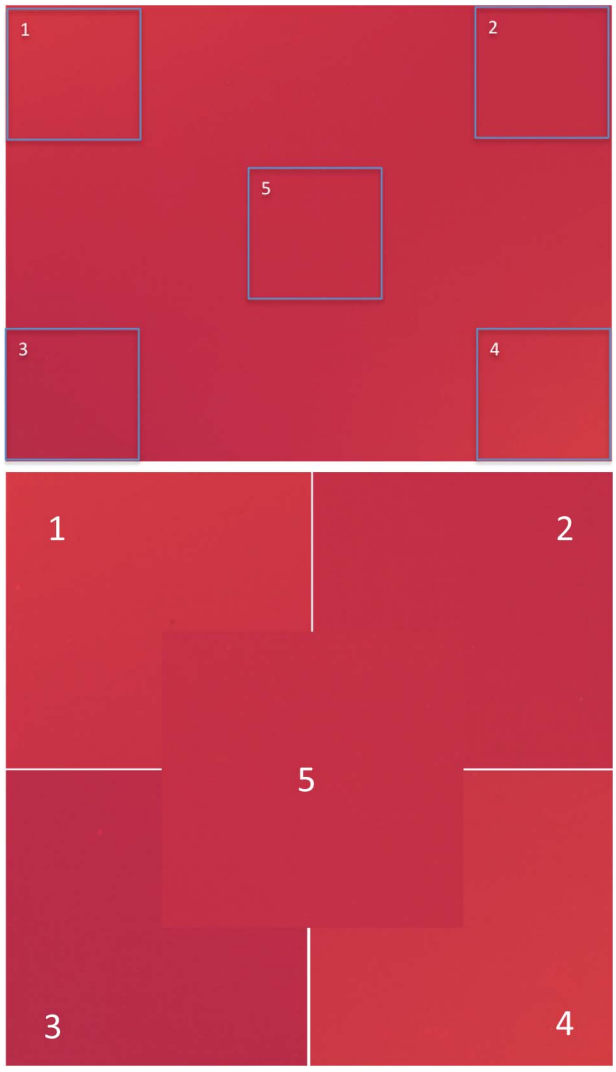

Fig. 2. Rendered image of a spatially uniform red paper using an LCTF imaging system.

calibrate the imaging system so it accurately measures spectral reflectance factor across the entire image plane.

3. IMAGING SYSTEM

The imaging system consisted of a 1.4 megapixel Lumenera LW165m monochrome camera utilizing a Sony ICX285 2/3 in. format 9.0 mm × 6.7 mm array sensor, a Kowa LM35XC 35 mm F 2.0 lens, and a wideband CRI Varispec LCTF positioned in front of the lens. Two Buhlite Sc-150 Soft Cube 150 W ceramic metal halide lamps were placed at 45° from the normal on either side of camera. These lights produced 4570 cd/m^2 with a correlated color temperature of 3857 K at the center of the object plane. Exposure time was optimized for each spectral band with the goal of achieving 50,000 counts of a maximum of 65,535 (i.e., 2^{16}–1) for a diffuse white. Twenty-nine spectral bands were captured between 420 and 700 nm. (For this particular setup, 400 and 410 nm resulted in excessive noise.) Ten images were

first taken with the lens cap on as an estimate of fixed-pattern noise, then averaged (referred to as "dark image"). Ten images were next captured of a sheet of Fluorilon, averaged, and low-pass spatial filtered to remove any surface defects and texture in the Fluorilon. All the images used to spatially correct and calibrate the system were an average of 10 successive images following dark-image subtraction and division by the Fluorilon image, also dark-image subtracted. Thus each image was corrected for fixed pattern noise and photometric inhomogeneity in both the lighting and imaging system. Previous experiments verified the photometric linearity of this system [5,6].

4. REFERENCE SPECTROPHOTOMETER

An X-Rite i1Pro spectrophotometer was used as the reference spectrophotometer. It was selected because it has bidirectional geometry, a small 4 mm measurement aperture, and a wavelength range greater than the LCTF. This instrument is used extensively in color-managed imaging because its measurement head just fits within calibration targets such as the X-Rite Digital ColorChecker SG and the X-Rite Passport. All recorded measurements were an average of four successive measurements with replacement.

5. WAVELENGTH-DEPENDENT SPATIAL CORRECTION

The system was first spatially corrected to account for chromatic errors resulting from the LCTF's sensitivity to changes in incident angle. Six sheets of uniform solid matte Color-aid paper mounted on a foam core were imaged: red, yellow, green, cyan, blue, magenta, and red. The absolute value of the CIELAB hue error, $|\Delta H^*_{ab}|$, was calculated for the entire sheet, comparing each pixel with the central pixel, shown in Fig. 3 for the cyan paper. The LCTF's angular sensitivity is readily seen where the hue error increases toward the edges. The cyan paper

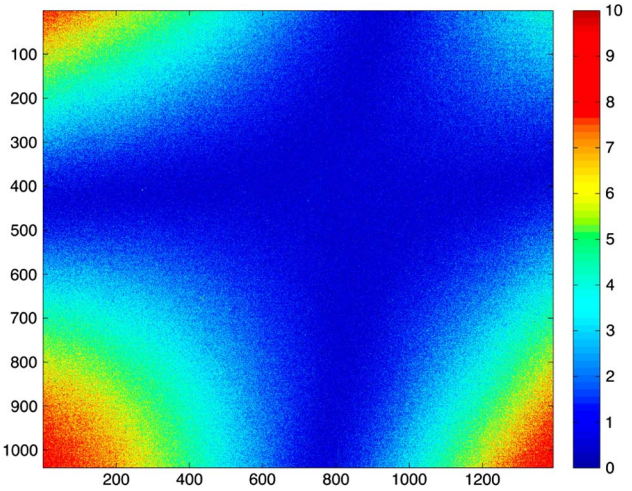

Fig. 3. Absolute value of CIELAB hue error for each pixel compared with the central pixel for the cyan Color-aid paper. Scale is 0–10$|\Delta H^*_{ab}|$.

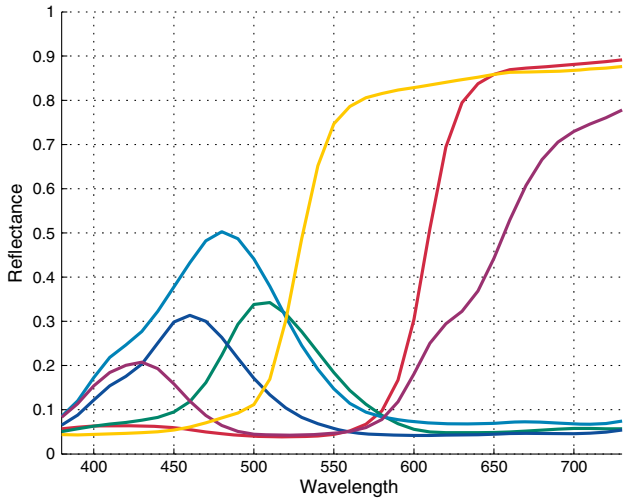

Fig. 4. Spectral reflectance factor measurements of the six Color-aid papers used for spatial correction.

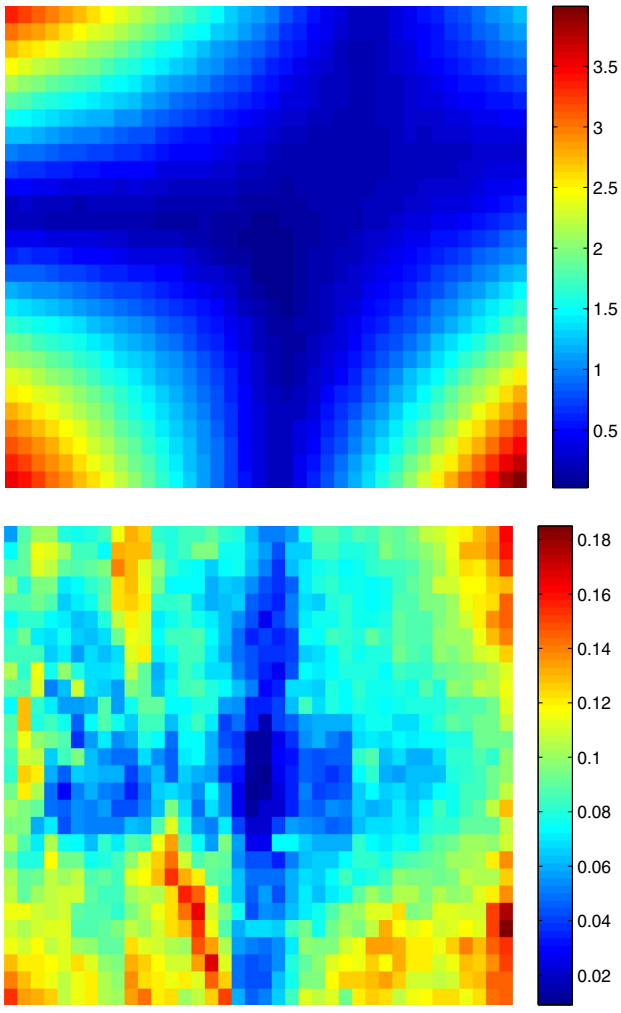

Fig. 5. Average CIEDE2000 of the six uniform color fields before (top) and after (bottom) spatial correction. Note the different scales.

Fig. 6. X-Rite Passport color target. Its size is approximately 17 cm × 12.5 cm.

showed the greatest sensitivity to the angular dependency. Berns and Reniff found similar sensitivity such that a cyan tile could be used to diagnose photometric and wavelength errors in reflectance spectrophotometry [12].

The measured spectral reflectance factor of the six colored papers using the reference spectrophotometer is plotted in Fig. 4. There was sufficient spectral variability and sample number to estimate the Eq. (2) model scalars. The optimization was automated by replacing a stepwise multiple-linear regression with a Moore–Penrose pseudo-inverse calculation (Matlab pinv) where the four scalars for the 29 spectral bands were estimated simultaneously. A potential problem with estimating scalars at each *xy* position is the introduction of image noise. Furthermore, it is computationally expensive. For this research, the image was divided into nine equal segments, and the average pixel data were used for the estimations. A two-dimensional quadratic function was fit to the nine segments' scalars so that banding artifacts would not be introduced and propagated between segments.

The 29 bands before and after spatial correction were used to render six colorimetric images for the 1931 standard observer and illuminant D65, corresponding to the six uniform colored papers. Each image was divided into 1200 (30 × 40) segments, and the CIEDE2000 total color difference was calculated comparing the average color of each segment to the central segment. The average of the six uniform colored papers is plotted in Fig. 5. Before correction the imaging system had very poor spatial uniformity. The bottom right corner led to a maximum color difference of 5.4 for the cyan paper. Following correction, the improvement was pronounced. The average CIEDE2000 for the combined papers reduced from 0.95 to 0.08, and the combined maximum reduced from 4.00 to 0.18. There remains a similar spatial pattern following correction, though at much smaller magnitude. Increasing the number of segments beyond nine would reduce this pattern. These model scalars only need to be calculated once for a specific imaging system. Each raw image would be spatially corrected before further processing.

6. SPECTRAL CALIBRATION

A target-based spectral calibration was performed using an X-Rite Passport color target, shown in Fig. 6. It contains 50 painted papers, 24 of them equivalent to an X-Rite ColorChecker Classic. The 24 samples were used to estimate model scalars for each spectral band. There were several advantages to using the Passport: it has appreciable spectral variability, a large number of samples (compared with calibrated tiles), and a small size, such that it can be included in all images. Before optimization, each spatially corrected band was considered a raw image, and lens cap and Fluorilon images were collected and used to again account for fixed-pattern noise and lighting inhomogeneity. This step was added to represent our actual workflow using this imaging system.

The results are listed in Table 1 both in units of CIEDE2000 and spectral reflectance factor RMS difference. The correction accounted for differences between the nominal and actual LCTF wavelength centroids and increasing bandwidth as a function of increasing wavelength. These results are excellent with average and maximum differences between the camera and reference spectrophotometer of 0.004 and 0.008 spectral reflectance factor RMS difference, respectively, and 0.45 (0.69) and 1.06 (1.57) CIEDE2000 (ΔE^*_{ab}). Similar results have been obtained when the analysis is repeated. As a comparison, the average performance for a X-Rite ColorChecker Classic imaged using an LCTF imaging system was an average and maximum of 0.243 and 0.729 spectral reflectance factor RMS difference, respectively, and 3.30 and 8.22 ΔE^*_{ab} [13].

The results are visualized in Fig. 7, where each square is divided into two triangles. The upper triangle is the LCTF measurement, and the lower triangle is the reference

Table 1. CIEDE2000 (ΔE^*_{ab}) and Spectral Reflectance Factor RMS Difference Values between the Reference Spectrophotometer and the LCTF Imaging System for the Calibration (X-Rite Passport) and Verification Targets

		CIEDE2000 ΔE^*_{ab}			Spectral RMS difference		
Target	Image	Mean	Max	90th per	Mean	Max	90th per
Calibration (Passport)	Raw image	8.01	11.95	10.13	0.112	0.323	0.193
	Calibrated	0.45 (0.69)	1.06 (1.57)	0.91 (1.3)	0.004	0.008	0.008
Verification	Raw image	10.68	17.67	15.08	0.153	0.333	0.271
	Calibrated	0.44 (0.63)	1.65 (2.34)	0.71 (1.12)	0.008	0.025	0.018

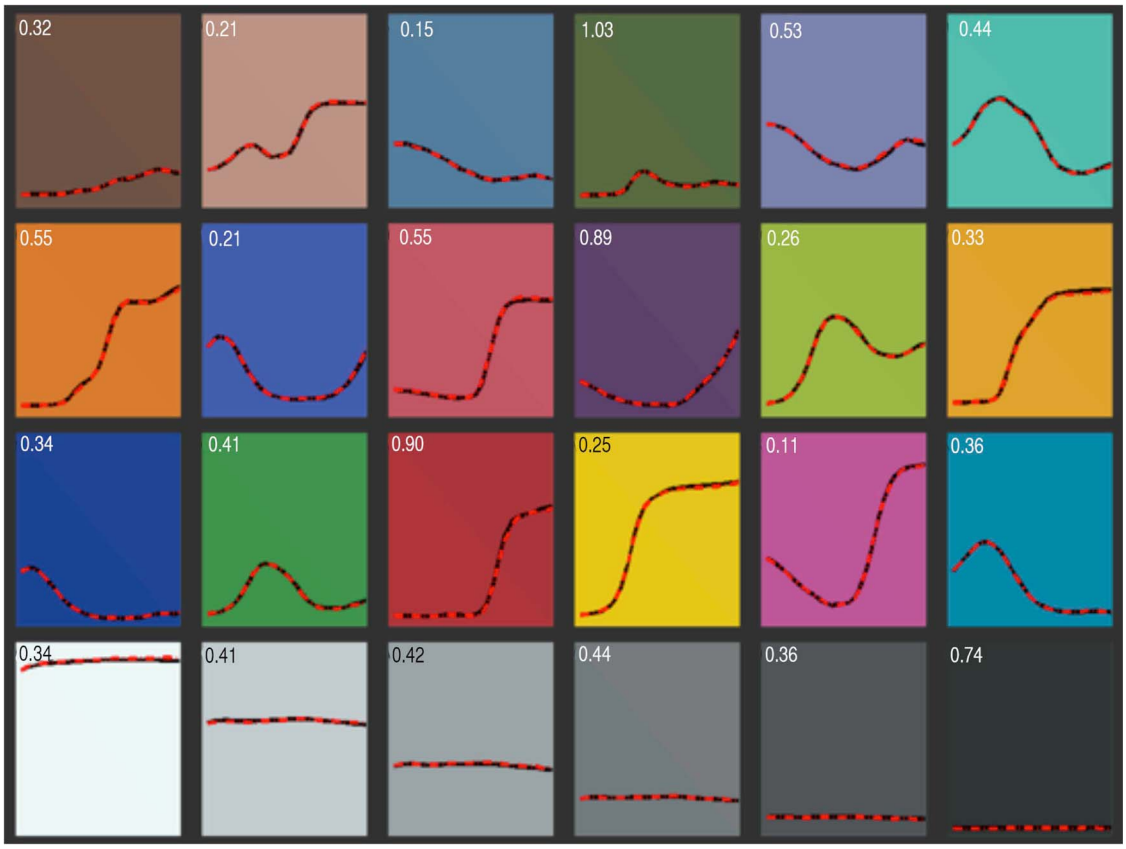

Fig. 7. Comparisons between reference spectrophotometer (black lines) and LCTF imaging system (dashed red lines) for the X-Rite Passport. The number in the upper left corner is the CIEDE2000. Each colored square is divided into two triangles where the upper and lower triangles correspond to the LCTF imaging system and reference spectrophotometer, respectively.

spectrophotometer measurements. For the majority of samples, these color differences are below the visual threshold in this visualization such that the triangles are not visible. The CIEDE2000 values are listed in the upper left corner. The spectral data are plotted where the LCTF measurements are shown as the dashed red lines and the reference spectrophotometer as black lines. Clearly the method is necessary in order to transfer the scale of the spectral reflectance factor to the imaging system.

Fig. 8. Custom verification color target. Its size is approximately 22 cm × 14.5 cm.

7. INDEPENDENT VERIFICATION

A custom target was used for independent verification, shown in Fig. 8. The color target contains 54 painted samples. There are three hue circles, each at different lightness levels. There are four gray scales: carbon black and either a bluish or yellowish white and two three-chromatic colorant scales. These many gray scales were created to test for subtle differences in color accuracy and to access observer metamerism between a camera and a CIE standard observer. The results are also listed in Table 1 and a visualization shown in Fig. 9. The accuracy remained the same as the Passport calibration target, verifying the methodology. The one exception was the black sample in which the imaging system resulted in a lower reflectance than the reference spectrophotometer. This was due to differences in measurement geometry between the imaging system and reference spectrophotometer and differences in gloss between the X-Rite Passport and the custom target. These geometry and gloss differences can be taken into account, particularly effective when materials requiring spectral imaging have very different gloss than the calibration target [14].

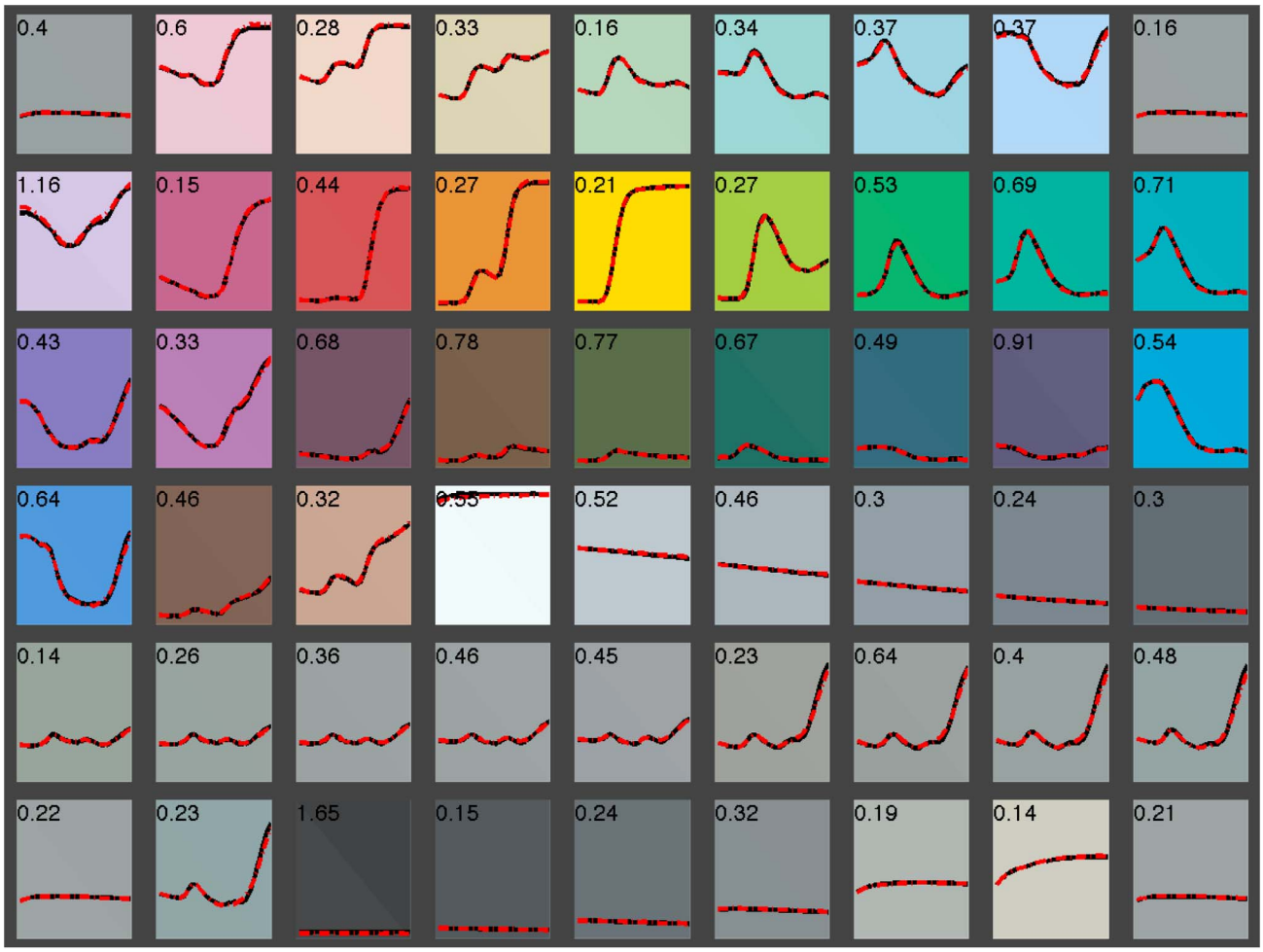

Fig. 9. Comparisons between reference spectrophotometer (black lines) and LCTF imaging system (dashed red lines) for the custom verification target. The number in the upper left corner is the CIEDE2000. Each colored square is divided into two triangles where the upper and lower triangles correspond to the LCTF imaging system and the reference spectrophotometer, respectively.

8. CONCLUSIONS

A statistical method of modeling and correcting systematic spectrophotometric errors in conventional reflectance spectrophotometry was successfully adapted to an LCTF imaging system. The model terms approximated photometric, wavelength, and bandwidth errors. The method corrected wavelength-dependent spatial inhomogeneity, previously assumed to be negligible. The method also transferred the scale of the spectral reflectance factor from a reference spectrophotometer to the imaging system with very low residual error.

A significant advantage of this approach is that each spectral band remains independent, reducing noise propagation [15] and potential registration errors, for example using interpolation to produce evenly spaced wavelength centroids or a single $\lambda \times \lambda$ calibration matrix, used previously in our research [16]. A final advantage is the use of a color target to transfer the scale of the spectral reflectance factor where only a single image is necessary.

Andrew W. Mellon Foundation.

David R. Wyble provided experimental assistance.

REFERENCES

1. H. R. Morris, C. C. Hoyt, and P. J. Treado, "Imaging spectrometers for fluorescence and Raman microscopy: acousto-optic and liquid crystal tunable filters," Appl. Spectrosc. **48**, 857–866 (1994).
2. N. Gat, "Imaging spectroscopy using tunable filters: a review," SPIE **4056**, 50–64 (2000).
3. D. W. Allen, M. Litorja, S. W. Brown, and Y. Zong, "Evaluation of a portable hyperspectral imager for medical imaging applications," SPIE **6765**, 67650F (2007).
4. Z. Khan, F. Shafait, and A. Mian, "Hyperspectral document imaging: challenges and perspectives," in *Camera-Based Document Analysis and Recognition: 5th International Workshop, CBDAR 2013, Washington, DC, USA, August 23, 2013, Revised Selected Papers*, M. Iwamura and F. Shafait, eds. (Springer, 2013), pp. 150–163.
5. B. Hensley and D. Wyble, "Spectral imaging using a liquid crystal tunable filter," Munsell Color Science Laboratory Technical Report, 2012, available at http://www.cis.rit.edu/DocumentLibrary/admin/uploads/CIS000196.pdf.
6. F. M. Abed and R. S. Berns, "Spectral imaging using a liquid crystal tunable filter—part II," Studio for Scientific Imaging and Archiving of Cultural Heritage, 2014, http://www.rit-mcsl.org/Mellon/PDFs/Abed_Berns_Spectral_Characterization_of_LCTF_p2.pdf.
7. E. A. Early and M. E. Nadal, "Uncertainty analysis for reflectance colorimetry," Color Res. Appl. **29**, 205–216 (2004).

8. E. A. Early and M. E. Nadal, "Uncertainty analysis for the NIST 0:45 reflectometer," Color Res. Appl. **33**, 100–107 (2008).
9. L. Reniff, "Transferring the 45/0 spectral reflectance factor scale," Color Res. Appl. **19**, 332–340 (1994).
10. A. R. Robertson, "Diagnostic performance evaluation of spectrophotometers," in *Advances in Standards and Methodology in Spectrophotometry*, C. Burgess and K. D. Mielenz, eds. (Elsevier, 1987), pp. 277–286.
11. R. S. Berns and K. H. Petersen, "Empirical modeling of systematic spectrophotometric errors," Color Res. Appl. **13**, 243–256 (1988).
12. R. S. Berns and L. Reniff, "An abridged technique to diagnose spectrophotometric errors," Color Res. Appl. **22**, 51–60 (1997).
13. J. Y. Hardeberg, F. Schmitt, and H. Brettel, "Multispectral color image capture using a liquid crystal tunable filter," Opt. Eng. **41**, 2532–2548 (2002).
14. F. M. Abed, R. S. Berns, and K. Masaoka, "Geometry-independent target-based camera colorimetric characterization," J. Imaging Sci. Technol. **57**, 50503 (2013).
15. P. D. Burns and R. S. Berns, "Error propagation analysis in color measurement and imaging," Color Res. Appl. **22**, 280–289 (1997).
16. R. S. Berns, "Color-accurate image archives using spectral imaging," in *Scientific Examination of Art: Modern Techniques in Conservation and Analysis* (The National Academies, 2005), pp. 105–119.